AD-A097 188 BOLT BERANEK AND NEWMAN INC CAMBRIDGE MA F/G 12/1
DETECTION THRESHOLDS FOR MULTI-TARGET TRACKING IN CLUTTER.(U)
JAN 81 T E FORTMANN, Y BAR-SHALOM, M SCHEFFE N00014-80-C-0270
UNCLASSIFIED BBN-4605 NL

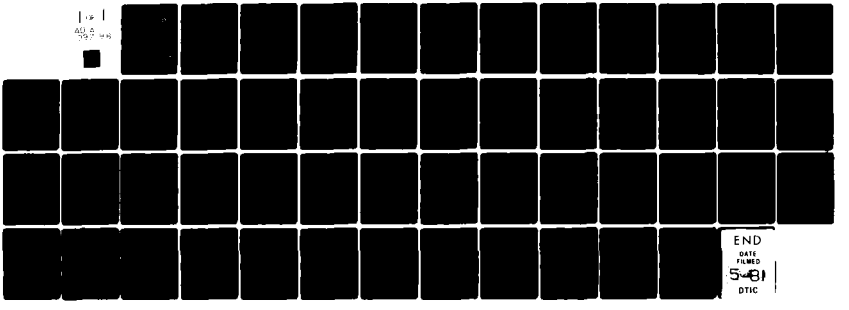

END
DATE FILMED
5-81
DTIC

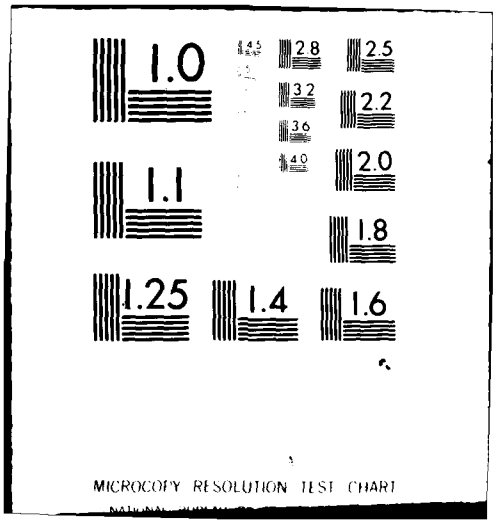
1.0
1.1
1.25
1.4
1.6
1.8
2.0
2.2
2.5
2.8
3.2
3.6
4.0
MICROCOPY RESOLUTION TEST CHART

Bolt Beranek and Newman Inc.

Report No. 4605

(5) LEVEL II

Detection Thresholds for Multi-Target Tracking in Clutter

Thomas E. Fortmann, Yaakov Bar-Shalom, and Molly Scheffe

January 1981

Contract N00014-80-C-0270
Task NR 274-310

Prepared for:
Naval Analysis Program
Office of Naval Research

Report No. 4605

DETECTION THRESHOLDS FOR MULTI-TARGET TRACKING IN CLUTTER

Thomas E. Fortmann, Yaakov Bar-Shalom, and Molly Scheffé

January 1981

Contract N00014-80-C-0270
Task NR 274-331

Prepared by:

Bolt Beranek and Newman Inc.
50 Moulton Street
Cambridge, Massachusetts 02238

Prepared for:

Naval Analysis Program
Office of Naval Research
800 North Quincy Street
Arlington, Virginia 22217

Attention: Mr. James G. Smith, Code 431

SECURITY CLASSIFICATION OF THIS PAGE (When Data Entered)

REPORT DOCUMENTATION PAGE	READ INSTRUCTIONS BEFORE COMPLETING FORM
1. REPORT NUMBER	2. GOVT ACCESSION NO. AD-A097 788 / 3. RECIPIENT'S CATALOG NUMBER
4. TITLE (and Subtitle) (6) DETECTION THRESHOLDS FOR MULTI-TARGET TRACKING IN CLUTTER	5. TYPE OF REPORT & PERIOD COVERED (9) Interim Report June - December 1980
	6. PERFORMING ORG. REPORT NUMBER BBN Report No. 4605
7. AUTHOR(s) (10) Thomas E. Fortmann, Yaakov Bar-Shalom, and Molly Scheffé	8. CONTRACT OR GRANT NUMBER(s) (15) N00014-80-C-0270
9. PERFORMING ORGANIZATION NAME AND ADDRESS Bolt Beranek and Newman Inc. 50 Moulton Street Cambridge, MA 02238	10. PROGRAM ELEMENT, PROJECT, TASK AREA & WORK UNIT NUMBERS 65152N NR 274-331
11. CONTROLLING OFFICE NAME AND ADDRESS (11) Naval Analysis Program (Code 431) Office of Naval Research Arlington, VA 22217	12. REPORT DATE January 1981
	13. NUMBER OF PAGES 49 (12) 57
14. MONITORING AGENCY NAME & ADDRESS(if different from Controlling Office) (14) BBN-4605	15. SECURITY CLASS. (of this report) UNCLASSIFIED
	15a. DECLASSIFICATION/DOWNGRADING SCHEDULE

16. DISTRIBUTION STATEMENT (of this Report)

Approved for public release; distribution unlimited

17. DISTRIBUTION STATEMENT (of the abstract entered in Block 20, if different from Report)

18. SUPPLEMENTARY NOTES

19. KEY WORDS (Continue on reverse side if necessary and identify by block number)

Detection thresholds	surveillance
multi-target tracking	clutter
data association	ROC curves
data correlation	tracking performance

20. ABSTRACT (Continue on reverse side if necessary and identify by block number)

Tracking performance depends upon the quality of the measurement data. In the Kalman-Bucy filter and other trackers, this dependence is well-understood in terms of the measurement noise covariance matrix, which specifies the uncertainty in the values of the measurement inputs. When the origin of the measurements is also uncertain, one has the widely-studied problem of data association (or data correlation), and tracking performance depends critically on additional parameters, primarily the

DD FORM 1 JAN 73 1473 EDITION OF 1 NOV 65 IS OBSOLETE

062200

SECURITY CLASSIFICATION OF THIS PAGE (When Data Entered)

20. ABSTRACT (continued)

probabilities of detection and false alarm. In this paper we derive a modified Riccati equation that quantifies (approximately) the dependence of the state error covariance on these parameters. We also show how to use an ROC curve in conjunction with the above relationship to determine an "optimal" detection threshold in the signal processing system that provides measurements to the tracker.

TABLE OF CONTENTS

LIST OF FIGURES

1. INTRODUCTION

Garden-variety tracking problems involve processing measurements (e.g., range and azimuth observed by a sensor) from a target of interest and producing, at each time step, an estimate of the target's current position and velocity vectors. Uncertainties in the target motion and in the measured values, usually characterized as random noise, lead to corresponding uncertainties in the target state.

A common and versatile approach to such problems involves assuming that the state dynamics and the measurements are both corrupted by additive, white, possibly Gaussian noise; the solution is then the celebrated Kalman-Bucy filter [1, 2, 3, 4, 5], which is the conditional mean state estimator, best linear estimator, maximum a posteriori estimator, maximum likelihood estimator, or least-squares estimator,[1] depending upon one's point of view. The parameters that determine tracking performance in such a filter are the system matrices in the equations describing target state dynamics and measurements, which will be considered fixed for the purposes of this discussion, and the covariance matrices of the process and measurement noise, which specify the uncertainties in target motion and measured values, respectively.

In many tracking problems, particularly those arising in surveillance, there is additional uncertainty regarding the origin of the received data, which may (or may not) include

---

[1] In the least-squares case, the assumptions about noise are replaced by assumptions about error weightings.

measurements from the target(s) of interest, interfering targets, or random clutter (false alarms). This leads to the problem of data association or data correlation, which has been attacked on a number of fronts [6, 7, 8, 9, 10, 11, 12, 13, 14] and surveyed in [15, 16, 17]. In this situation, tracking performance depends not only upon the noise covariances, but upon the amount of uncertainty in measurement origin. In some of the approaches cited above [6, 7, 8, 9, 10], this dependence is explicit and is characterized in terms of the detection probability and clutter density (which is proportional to false alarm probability).

In typical applications, measurement data are provided to a tracker by upstream signal processing and detection algorithms, as indicated in Figure 1. The process noise covariances are normally selected on the basis of experience and intuition (i.e., they are guessed). The measurement noise covariances are either provided by the signal processing algorithm, as shown in the figure, or they are selected in the same manner as the process noise. In any case, the true noise levels are usually fixed by target dynamics and sensor configuration and cannot be adjusted on line.

Detection and false alarm probabilities, on the other hand, are highly interdependent and adjustable via a detection threshold: raising the threshold lowers both probabilities, and vice-versa. This relationship, which is also parameterized by signal-to-noise ratio (SNR), is usually characterized by means of a set of receiver operating characteristic (ROC) curves, as discussed below in Section 4. The threshold is typically set by choosing a design point on the most applicable ROC curve, based on the perceived tradeoffs between false alarms and missed detections. However, to the best of our knowledge, these tradeoffs have never included any systematic or quantitative

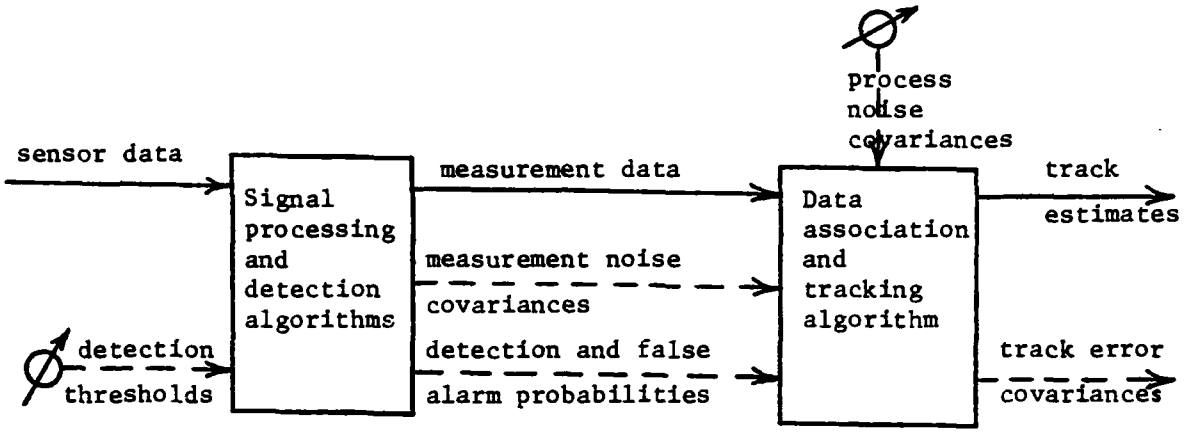

FIG. 1. TRACKING SYSTEM BLOCK DIAGRAM

consideration of the effects downstream on data association and tracking performance.

In this paper we shall derive such a quantitative relationship, in which the dependence of a tracker's error covariance upon detection and false alarm probability is explicitly (but approximately) characterized by a scalar parameter in the covariance equation (modified Riccati equation). This result is important for the following reasons:

1. Contour plots of the scalar parameter as a function of detection probability and false alarm probability form a set of "tracker operating characteristic" (TOC) curves, which can be superimposed on ROC curves for the detector or receiver of interest in order to determine graphically the operating point that "optimizes" tracker performance.

2. The stability of the tracking process depends

critically on the detection and false alarm probabilities; whether the modified Riccati equation remains stable for all values of the scalar parameter remains an open question.

3. Allocation of tracking resources (both computation and communication) requires prediction of future state error covariances under various resource configurations, i.e., as a function of detection and false alarm probability and of process and measurement noise covariance.

4. The same derivations provide a solution to the related problem of determining the statistical properties of the modified likelihood function [18], used for decision making (e.g. maneuver detection) when measurement origins are uncertain.

In Section 2 the problem of relating tracking performance to detection and false alarm probabilities is formulated in the context of probabilistic data association. The key results are derived in the next section, followed by analyses and ROC curves of simple receivers in Section 4. These results are combined in Section 5 and used to select optimal operating points on the ROC curves. Application to the modified likelihood function is discussed in the next section, followed by concluding remarks in Section 7.

2. PROBLEM FORMULATION

Consider a dynamic system (target model) of the usual form,

$$\underline{x}_{k+1} = \underline{F}\underline{x}_k + \underline{G}\underline{w}_k \tag{1}$$

$$\underline{y}_k = \underline{H}\underline{x}_k + \underline{v}_k \tag{2}$$

where $\underline{x}$ is the state vector, $\underline{y}$ is the measurement vector, $\underline{w}$ and $\underline{v}$ are zero-mean, mutually independent, white, gaussian noise vectors with covariance matrices $\underline{Q}$ and $\underline{R}$, respectively, and k is a discrete time index. The matrices $\underline{F}$, $\underline{G}$, $\underline{H}$, $\underline{Q}$, and $\underline{R}$ are assumed known and their dependence on t is suppressed here for notational convenience. The initial state is assumed gaussian with mean $\hat{\underline{x}}_{0|0}$ and covariance $\underline{P}_{0|0}$. A typical state vector would include position and velocity variables, as well as other information that relates to the specific type of platform being tracked, and typical dynamics would assume straight-line or great-circle target motion with disturbances from the process noise $\underline{w}$.

The tracker's estimate of the target state $\underline{x}_k$ at time k, given data up to time i, is denoted $\hat{\underline{x}}_{k|i}$. The error in this estimate is $\tilde{\underline{x}}_{k|i} = \underline{x}_k - \hat{\underline{x}}_{k|i}$, with error covariance matrix $\underline{P}_{k|i} = E\{\tilde{\underline{x}}_{k|i}\tilde{\underline{x}}'_{k|i}\}$, where E denotes expectation. The discrete-time Kalman-Bucy filter [2, 3, 4, 5] propagates these in two stages. The prediction stage accounts for time evolution,

$$\hat{\underline{x}}_{k|k-1} = \underline{F}\hat{\underline{x}}_{k-1|k-1} \tag{3}$$

$$\underline{P}_{k|k-1} = \underline{F}\underline{P}_{k-1|k-1}\underline{F}' + \underline{G}\underline{Q}\underline{G}' \tag{4}$$

starting from the initial conditions $\underline{\hat{x}}_{0|0}$ and $\underline{P}_{0|0}$. The update stage compares the incoming measurement $\underline{y}_k$ with the predicted measurement $\underline{\hat{y}}_k = \underline{H}\underline{\hat{x}}_{k|k-1}$ to form the innovation vector

$$\underline{\tilde{y}}_k \triangleq \underline{y}_k - \underline{\hat{y}}_{k|k-1} \tag{5}$$

whose covariance matrix is

$$\underline{S}_k \triangleq E\{\underline{\tilde{y}}_k \underline{\tilde{y}}_k'\} = \underline{H}\underline{P}_{k|k-1}\underline{H}' + \underline{R} \tag{6}$$

The state and covariance are then updated via

$$\underline{\hat{x}}_{k|k} = \underline{\hat{x}}_{k|k-1} + \underline{W}_k \underline{\tilde{y}}_k \tag{7}$$

$$\begin{aligned} \underline{P}_{k|k} &= (\underline{I} - \underline{W}_k\underline{H})\underline{P}_{k|k-1}(\underline{I} - \underline{W}_k\underline{H})' + \underline{W}_k\underline{R}\underline{W}_k' \\ &= \underline{P}_{k|k-1} - \underline{W}_k\underline{S}_k\underline{W}_k' \end{aligned} \tag{8}$$

where $\underline{W}_k \triangleq \underline{P}_{k|k-1}\underline{H}'\underline{S}_k^{-1}$ is the gain matrix. The resulting state estimate, under the above assumptions, is the <u>conditional mean</u> $\underline{\hat{x}}_{k|k} = E\{\underline{x}_k | Y^k\}$ where Y^k denotes all data vectors $\underline{y}_i$ for $i \leq k$.

In order to avoid clouding the discussion to follow, this brief summary ignores a number of complications that arise in practice. If the system is nonlinear, for example, then it can usually be linearized and the same basic equations can be applied to deviations from the nominal trajectory [3, 5]. If the target occasionally deviates from the assumed motion model, e.g., by maneuvering, then some decision-making or other machinery must be provided to deal with these instances.

In multi-sensor problems, the size and composition of the

measurement vector often varies from one time to the next; in other words, $\underline{y}_k$ is composed of independent subvectors from various sensors, any subset of which may be present at a given time. Moreover, in the problem of interest here, each sensor supplies not one but several subvectors that must be associated with targets. We will avoid the resulting notational morass by restricting equations (5)-(8) to apply to a measurement subvector $\underline{y}_k$ from a single sensor. In addition, we will suppress the time subscript k from all variables except $\underline{P}$ and Y, unless it is required for clarity. Without any loss of generality, the data association problem may now be formulated as follows.

At each time step, the sensor provides a set of candidate measurements to be associated with targets (or rejected). In most approaches, this is done by forming a "validation gate" around the predicted measurement from each target and selecting those detections that lie within the gate. There are many different approaches to establishing a correspondence between candidate measurements and targets; some of these were cited above in Section 1.

In this paper we shall focus on the probabilistic data association (PDA) method [6, 7, 15], although the results are relevant to other methods [9, 10] in which similar machinery is used. The m candidate measurements are denoted $\underline{y}_j$, j=1,...m, and their corresponding innovations are

$$\tilde{\underline{y}}_j \triangleq \underline{y}_j - \hat{\underline{y}}, \qquad j=1,...m \tag{9}$$

The term measurement will be used interchangeably for $\underline{y}_j$ and $\tilde{\underline{y}}_j$, since they contain equivalent information [5].

Considering a single target independently of any others, χ_j

denotes the event that the j-th measurement belongs to that target and χ_0 the event that none of the measurements belongs to it (no detection). The PDA approach builds upon the assumptions that the estimation errors $\tilde{\underline{x}}$ and $\tilde{\underline{y}}$ have gaussian densities at each time step (this is approximate, since there is an exponentially growing tree of possible measurement sequence hypotheses and the true densities are weighted sums of gaussians). It is also assumed that the correct measurement is detected with probability P_D (independently at each time) and that all other measurements are Poisson-distributed[2] with parameter CV, where C is the expected number of false measurements per unit volume and V is the volume of the validation gate.

The gate is normally a g-sigma ellipsoid $\{\tilde{\underline{y}} : \tilde{\underline{y}}'\underline{S}^{-1}\tilde{\underline{y}} \leq g^2\}$ and P_G is the probability that the correct measurement, if detected, lies within the gate.[3] The gate volume is thus $V = c_M g^M |\underline{S}|^{1/2}$, where M is the dimension of $\tilde{\underline{y}}$ and $c_M = \pi^{M/2}/\Gamma(M/2+1)$ is the volume of the M-dimensional unit sphere ($c_1=2$, $c_2=\pi$, $c_3=4\pi/3$, etc.).

The conditional mean estimate $\hat{\underline{x}}$ is obtained from (7) by using the combined (weighted) innovation

$$\tilde{\underline{y}} \triangleq \sum_{j=1}^{m} \beta_j \tilde{\underline{y}}_j \qquad (10)$$

---

[2]Equivalently, the number n of false measurements has probability mass function $p(n) = e^{-CV}(CV)^n/n!$ and the location of each false measurement is uniformly distributed in the gate.

[3]This is just the gaussian probability mass in the gate, which is often assumed to be unity in practice, since $P_G > .99$ whenever $g > M^{1/2}+2$.

where $\beta_j \triangleq P\{\chi_j | Y^k\}$, j=0,1,...m, is the posterior probability that the j-th measurement (or no measurement, for j=0) is the correct one. These probabilities are given by the following expressions (see Appendix A):

$$\beta_j = \frac{\exp(-\tilde{\underline{Y}}_j' \underline{S}^{-1} \tilde{\underline{Y}}_j / 2)}{b + \sum_{i=1}^{m} \exp(-\tilde{\underline{Y}}_i' \underline{S}^{-1} \tilde{\underline{Y}}_i / 2)}, \quad j=1,...m \tag{11}$$

$$\beta_0 = \frac{b}{b + \sum_{i=1}^{m} \exp(-\tilde{\underline{Y}}_i' \underline{S}^{-1} \tilde{\underline{Y}}_i / 2)} \tag{12}$$

where

$$\begin{aligned} b &\triangleq (2\pi)^{M/2} C |\underline{S}|^{1/2} (1-P_D P_G)/P_D \\ &= (2\pi)^{M/2} (CV/c_M g^M)(1-P_D P_G)/P_D \end{aligned} \tag{13}$$

The covariance update equation (8) becomes

$$\underline{P}_{k|k} = \underline{P}_{k|k-1} - (1-\beta_0)\underline{WSW}' + \underline{P}_k \tag{14}$$

where

$$\underline{P}_k \triangleq \underline{W}[\sum_{j=1}^{m} \beta_j \tilde{\underline{Y}}_j \tilde{\underline{Y}}_j' - \tilde{\underline{Y}}\tilde{\underline{Y}}']\underline{W}' \tag{15}$$

The data-dependent factors β_0 and $\underline{P}_k$ transform the original deterministic Riccati equation into a stochastic one.

The principal purpose of this paper is to explore the dependence of tracking performance, particularly the behavior of $\underline{P}_{k|k}$, on detection probability P_D and clutter density C. This is accomplished in the next section by means of a deterministic approximation to the stochastic modified Riccati equation (14).

Another major problem in data association and tracking is the testing of hypotheses for maneuver detection, track initiation, signature formation, target classification, and other decision-making purposes. The uncertainty in measurement origin leads, in the PDA and other approaches, to a modified likelihood function [18] involving the combined innovation $\underline{\tilde{y}}$ in (10). A major drawback of this approach was the difficulty of computing the covariance matrix of $\underline{\tilde{y}}$, but this can now be done using an intermediate result to be derived in the next section. Its application to the modified likelihood function will be discussed in Section 6.

Finally, note that multiple targets can be handled simultaneously via the joint probabilistic data association (JPDA) approach [8], in which the posterior probabilities (11)-(12) are computed jointly across a set of potentially interfering targets. Although this is a very important extension, it greatly complicates the derivations and will not be included here.

3. APPROXIMATE COVARIANCE EQUATION

Since any measure of tracking performance must depend heavily (or perhaps exclusively) on the error covariance matrix $\underline{P}_{k|k}$, we shall attempt to characterize its behavior in the presence of uncertainties in measurement origin. $\underline{P}_{k|k}$ is a random (data-dependent) matrix governed by the nonlinear, stochastic difference equations (4) and (14), and hence its behavior can only be determined in a statistical sense. Moreover, even propagation of its first and second moments appears to be intractable except via extensive numerical operations.

Consequently, we shall consider an approximation to (14) in which the random matrix $\underline{P}_k$ defined in (15) and the probability β_0 given by (12) are replaced by their (prior) expected values

$$\underline{P}_k = E\{\underline{P}_k | Y^{k-1}\} \tag{16}$$

$$\bar{\beta}_0 = E\{\beta_0 | Y^{k-1}\} = E\{\beta_0\} = 1 - P_D P_G \tag{17}$$

where the final expression is a consequence of $E[P\{A|B\}] = P\{A\}$.

These substitutions make (4) and (14) into a set of deterministic equations that can be iterated forward in time. Because (14) is nonlinear in $\underline{P}_{k|k-1}$, this does not yield $E\{\underline{P}_{k|k}\}$; nevertheless, it will give approximate values of future state error covariances in the presence of uncertain detections and false alarms as a function of the environmental parameters P_D and C, and of the noise covariances $\underline{R}$ and $\underline{Q}$.

Expansion of (16) yields

$$\underline{P}_k = E\{\underline{P}_k|Y^{k-1}\} = E\{E[\underline{P}_k|m,Y^{k-1}]|Y^{k-1}\}$$

$$= \sum_{m=0}^{\infty} E[\underline{P}_k|m,Y^{k-1}]P\{m|Y^{k-1}\} \tag{18}$$

where $P\{m|Y^{k-1}\} = P\{m\}$ is given by (37) in Appendix A. Using (15) and (10), the inside expectation becomes

$$E[\underline{P}_k|m,Y^{k-1}] = \begin{cases} \underline{W}[\underline{U}_1(m)-\underline{U}_2(m)]\underline{W}', & m=1,2,\ldots \\ 0, & m=0 \end{cases} \tag{19}$$

where

$$\underline{U}_1(m) \triangleq E[\sum_{i=1}^{m} \beta_i \underline{\tilde{y}}_i \underline{\tilde{y}}_i'|m,Y^{k-1}] \tag{20}$$

and[4]

$$\underline{U}_2(m) \triangleq E[\sum_{i=1}^{m} \beta_i \underline{\tilde{y}}_i \sum_{j=1}^{m} \beta_j \underline{\tilde{y}}_j'|m,Y^{k-1}]$$

$$= E[\sum_{i=1}^{m} \beta_i^2 \underline{\tilde{y}}_i \underline{\tilde{y}}_i'|m,Y^{k-1}] \tag{21}$$

The expected values are obtained by multiplying the quantities in square brackets by the joint prior density $p(\underline{\tilde{y}}_1,\ldots\underline{\tilde{y}}_m|m,Y^{k-1})$ given in (42) and integrating over the validation gate.

---

[4]The second expression in (21) is obtained as a intermediate result in Appendix B.

Considerable simplifications result if one applies a linear transformation of variables ($\underline{S}^{-1/2}$) to obtain a spherical gate, followed by a change to spherical coordinates. Because of the spherical symmetry of the gaussian density and of the expressions (20)-(21), off-diagonal elements, cross-terms, and angular variables drop out like flies, leaving scalar integrals over the radial variables (i.e., over $||\underline{Y}_j||$, j=1,...m). The detailed derivation, which is given in Appendix B, leads to

$$\underline{U}_1(m) = m \frac{P_D}{P_D P_G m + (1-P_D P_G)CV} \frac{c_M}{(2\pi)^{M/2}} I_1 \underline{S} \tag{22}$$

$$\underline{U}_2(m) = m \frac{P_D}{P_D P_G m + (1-P_D P_G)CV} \frac{c_M}{(2\pi)^{M/2}} \left(\frac{M}{g^M}\right)^{m-1} I_2(m) \underline{S} \tag{23}$$

where the scalar integrals I_1 and $I_2(m)$ are defined as

$$I_1 \triangleq \int_0^g r^{M+1} \exp(-r^2/2)\, dr \tag{24}$$

$$I_2(m) \triangleq \int_0^g \cdots \int_0^g \frac{\exp(-r_1^2)\, r_1^2}{b + \sum_{j=1}^{m} \exp(-r_j^2/2)} (r_1 r_2 \cdots r_m)^{M-1} dr_1 \cdots dr_m \tag{25}$$

and the constant b is defined in (13).

Substituting (22)-(25) and (37) into (18) and cancelling leads to

$$\underline{P}_k = (q_1 - q_2)\underline{WSW}' \tag{26}$$

where

$$q_1 \triangleq P_D \frac{c_M}{(2\pi)^{M/2}} \sum_{m=1}^{\infty} \frac{e^{-CV}(CV)^{m-1}}{(m-1)!} I_1 = P_D \frac{c_M}{(2\pi)^{M/2}} I_1 \tag{27}$$

$$q_2 \triangleq P_D \frac{c_M}{(2\pi)^{M/2}} \sum_{m=1}^{\infty} \frac{e^{-CV}(CV)^{m-1}}{(m-1)!} \left(\frac{M}{g^M}\right)^{m-1} I_2(m) \tag{28}$$

and substitution of this and (17) into (14) yields

$$\underline{P}_{k|k} = \underline{P}_{k|k-1} - (P_D P_G - q_1 + q_2)(\underline{WSW}') \tag{29}$$

This can be simplified further by noting that for typical values of g and M (g=4 or 5 and M<10), P_G is approximately 1 and q_1 is approximately P_D (substitute $x^{1/2}$ for r in I_1 to get a gamma function).

The upshot of all this is that the deterministic approximation to the covariance equation becomes

$$\underline{P}_{k|k} = \underline{P}_{k|k-1} - q_2(\underline{WSW}') \tag{30}$$

where the scalar parameter q_2, defined in (28), depends on P_D and C and lies between 0 and 1. Comparing this to (8), it is clear that the factor q_2 reduces the covariance improvement due to the term $\underline{WSW}'$: the smaller q_2 is, the greater the degradation. Thus, q_2 provides a useful measure of tracking performance as a function of P_D and C.

Evaluation of q_2

A Monte Carlo integration program has been used to integrate (25) and compute q_2 for various values of P_D and C. Evaluating the integrand in (25) at 5000 random points and truncating the sum in (28) at 10 terms yields a table of q_2 values with error standard deviations of 0.5-1.5% for M=1 and 2, and 1-5% for M=3.

It is useful to display these numbers via contour plots of q_2, as shown in Figures 2-4 (the curves become smoother if more points are used in the Monte Carlo integration). The vertical axis is P_D and the horizontal axis is CV, the expected number of false measurements in the gate (proportional to false alarm probability). A 4-sigma gate (g=4) was used and the three plots correspond to measurement vectors $\underline{y}$ with dimensions M = 1, 2, and 3, respectively. We shall refer to these as <u>tracker operating characteristic</u> (TOC) curves, by analogy with the receiver operating characteristic (ROC) curves to be given in Section 4 below.

Note that $V = c_M g^M |\underline{S}|^{1/2}$ and $\underline{S} = \underline{H}\underline{P}_{k|k-1}\underline{H}' + \underline{R}$, so that the gate volume in fact depends upon the state error covariance matrix $\underline{P}_{k|k-1}$. It follows that the above analysis is fully valid only in steady state ($\underline{P}_{k|k-1} \approx$ constant). We are currently working on extending this procedure by iterating equations (4), (30), and (28) to obtain $\bar{\underline{P}}(P_D,C)$, the steady-state error covariance matrix. A slightly modified set of TOC curves can then be formed with $|\bar{\underline{P}}|^{1/2}$ (or some other appropriate metric) plotted as a function of P_D and C. In the process of obtaining the table of $\bar{\underline{P}}(P_D,C)$, we also expect to determine empirically those values of P_D and C for which the covariance equations become unstable.

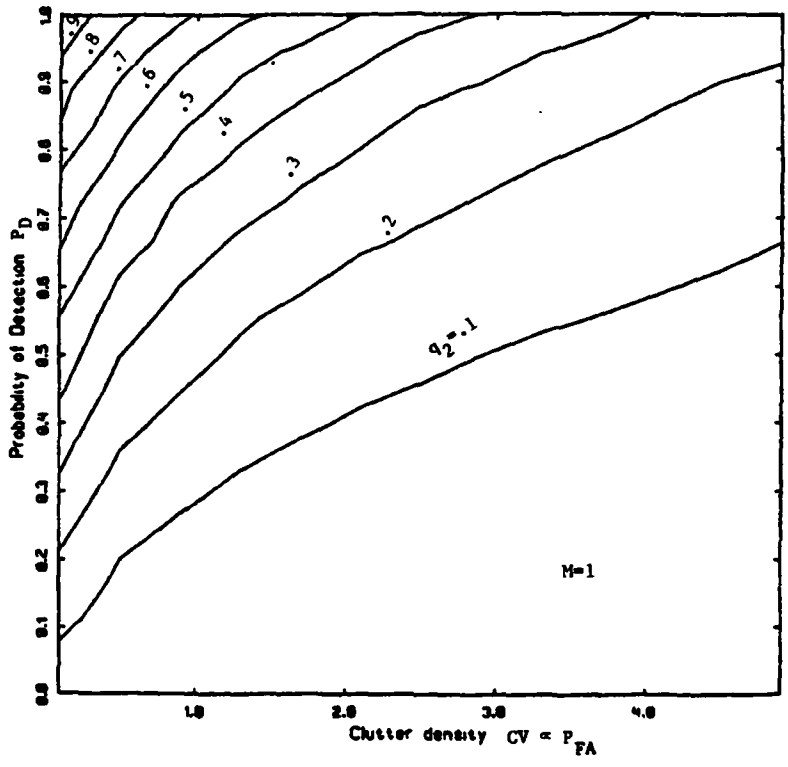

FIG. 2. TRACKER OPERATING CHARACTERISTICS FOR M=1

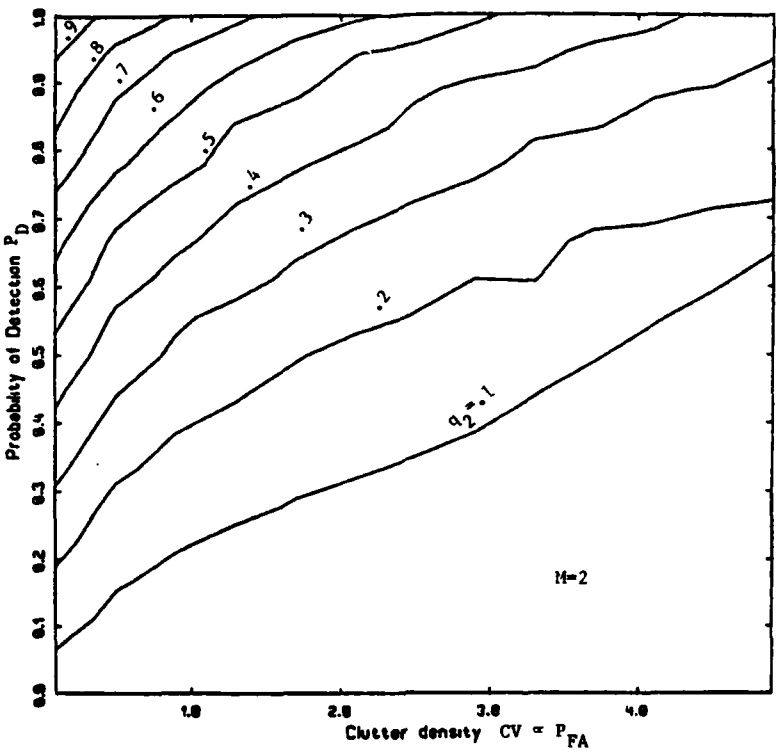

FIG. 3. TRACKER OPERATING CHARACTERISTICS FOR M=2

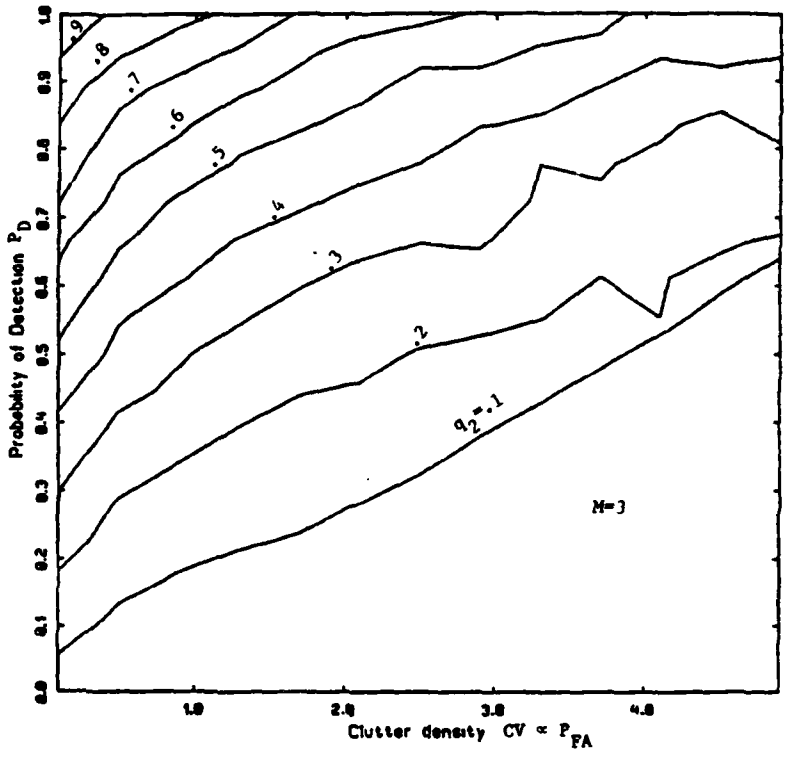

FIG. 4. TRACKER OPERATING CHARACTERISTICS FOR M=3

4. ANALYSIS OF DETECTION ALGORITHMS

The tracking inputs shown in Figure 1 can come from a variety of sources, ranging from simple threshold detectors to complex, multi-dimensional signal processing algorithms. Nevertheless, it is often possible to view the source of measurement data as a classic receiver structure in which a threshold level and/or other parameters control the probabilities of detection (P_D) and false alarm (P_{FA}).

In passive sonar applications, for example, time series data from each sensor is often passed through a beamformer, resulting in several data streams (beams) corresponding to different angles of arrival (azimuths), and then a sequence of fast Fourier transforms (FFTs) is performed on each data stream. The FFT operation may be viewed as a bank of filters, so that one deals with many separate narrowband time series, one from each beam-bin or resolution "cell" in the two-dimensional frequency-azimuth space.

There are many different detection algorithms for dealing with these data streams; their structures depend upon the nature of the application and the expected signals. A simple but common procedure, if the signals are narrowband and relatively stable, is to form power spectra (i.e., take the squared magnitude of each sample) and then integrate (i.e., sum) each data stream over an appropriate period of time. At the end of each integration period, a noise spectrum equalization (NSE) procedure compensates for different background noise levels at different frequencies, and detections are declared in all beam-bins for which the integrated output exceeds a threshold.

Except for the NSE, this amounts to passing each data stream

through an energy detector [19, 20], which assumes an unknown signal in white, gaussian noise. Under the noise-only hypothesis, the test statistic has a chi-square distribution with 2TW degrees of freedom, where T is the integration time and W is the bin width. With the signal present, it has a non-central chi-square distribution with the same degrees of freedom and non-centrality parameter equal to the SNR.

We shall use these distributions to compute receiver operating characteristics (ROCs). A standard ROC curve is the locus of points (P_{FA}, P_D) obtained as the detection threshold varies over all possible settings, and a family of such curves for different SNRs is usually plotted.

In this case an energy detector is operating on each frequency-azimuth cell, and we are interested in the expected number of false alarms in all cells of interest, which is the single-cell false alarm probability multiplied by the number of independent cells in a tracker's validation gate. Most algorithms require detections to be separated by one or more empty cells (i.e., adjacent cells above threshold are considered part of the same detection), and the effective number of cells generally depends in a complicated way on the details of the algorithm. For the sake of this discussion, we shall simply assume that false alarms can potentially occur in 1/3 of the cells in any given integration period.

A typical automatic line detection algorithm of the type described above might have an integration time of 250 sec. and FFT resolution of 0.1 Hz, or 50 degrees of freedom, and each cell would be 1 beam by 0.1 Hz. The tracker in this situation might have an innovation covariance matrix

$$\underline{S} = \begin{bmatrix} 1 \text{ beam} & 0 \\ 0 & 0.3 \text{ Hz} \end{bmatrix}^2 \qquad (31)$$

and a 4-sigma validation gate with volume

$$V = c_2 g^2 |\underline{S}|^{1/2} = \pi(16)(0.3) \approx 15 \text{ beam-Hz} \qquad (32)$$

The total number of resolution cells in the gate is thus 15/0.1 = 150, and the number of independent cells is 150/3 = 50. It follows that the expected number of false alarms per gate is $CV = 50P_{FA}$.

A set of ROC curves for an energy detector, computed using the above assumptions, is shown in Figure 5. For a given SNR, one can adjust the detection threshold so as to select an operating point anywhere along the corresponding ROC curve.

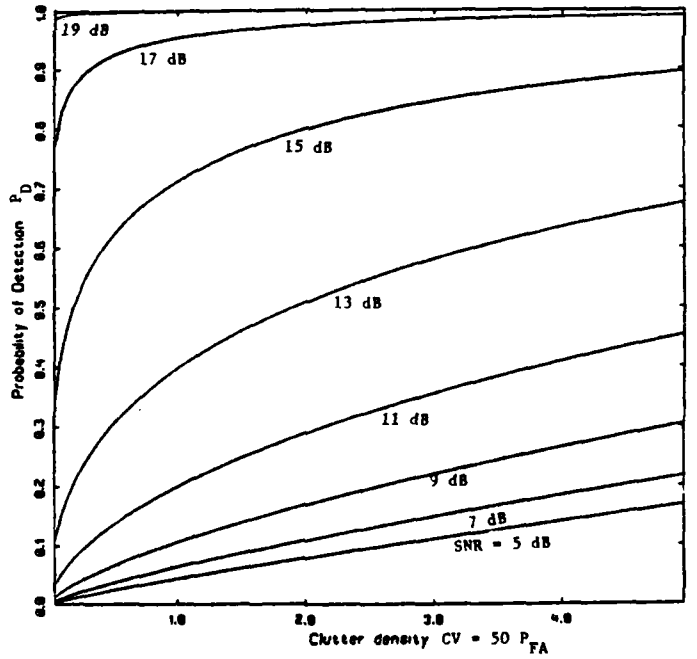

FIG. 5. TYPICAL ROC CURVES FOR ENERGY DETECTOR

More sophisticated narrowband line detectors and line

trackers utilize complex spectra, and their effective integration times are usually less than those described above. Although the details of these algorithms vary greatly, their basic operations tend to be similar to those of a quadrature receiver or incoherent matched filter [20], which assumes a sinusoidal signal of unknown phase. Under the signal-plus-noise hypothesis, the test statistic has a Rician distribution, which reduces to a Rayleigh distribution in the noise-only case.

A set of ROC curves for a quadrature receiver is shown in Figure 6. These were computed using the expressions given in [20] for P_{FA} and P_D, and using the same validation gate as above. Another set, for the case where both amplitude and phase are unknown (slow Rayleigh fading), is shown in Figure 7.

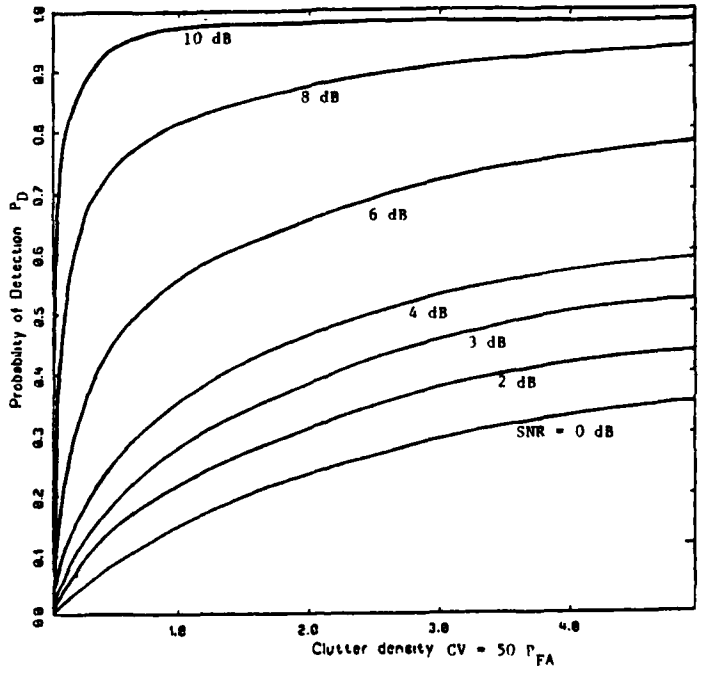

FIG. 6. ROC CURVES FOR QUADRATURE RECEIVER

Another class of algorithms for passive sonar applications

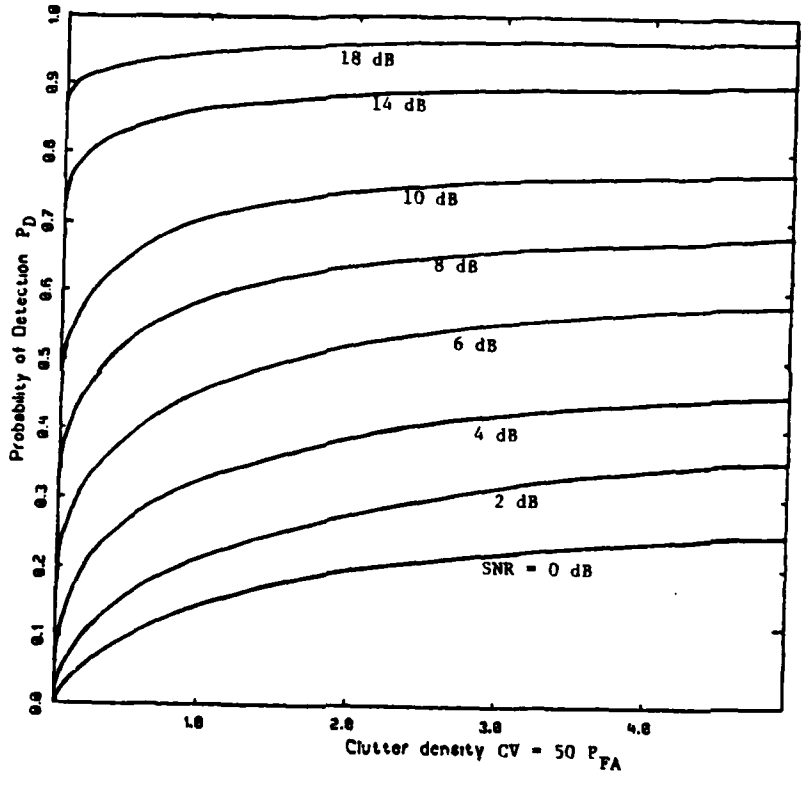

FIG. 7. ROC CURVES FOR QUADRATURE RECEIVER WITH RAYLEIGH FADING

involves coherent or incoherent correlation of data received at two geographically distinct sites. The resulting statistic, as a function of time delay and frequency (Doppler) shift, is known as an ambiguity surface, and a signal received at both sites from the same target produces a peak in the surface. Detection of peaks above some threshold is qualitatively similar to the situation described above, in which peaks are sought in the frequency-azimuth plane. With appropriate assumptions, approximate ROC curves can be obtained for such receivers.

5. OPTIMIZATION OF TRACKING PERFORMANCE

Superimposing one of the sets of TOC contours from Figures 2-4 on one of the ROC curves from Figures 5-7, an operating point (i.e., threshold) can be selected so as to maximize q_2 and "optimize" tracking performance. For example, Figure 8 shows the TOC contours for M=2 superimposed on the ROC curve corresponding to a quadrature receiver and SNR = 8 dB. The "optimal" point is indicated by ⊗.

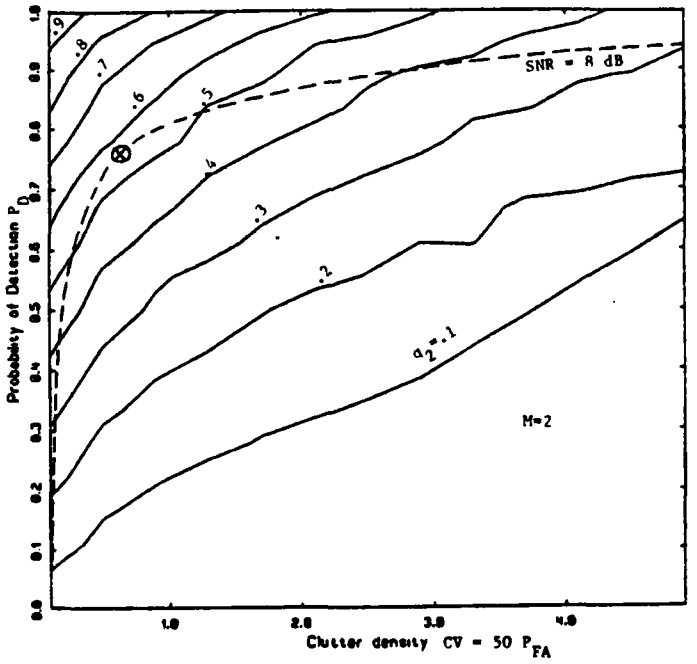

FIG. 8. OPTIMAL THRESHOLD SETTING FOR QUADRATURE RECEIVER WITH SNR = 8 DB

This graphical method for selecting an operating point can, of course, be replaced by a mathematical optimization; the obvious necessary condition is that the ROC and TOC curves be tangent. However, the practical difficulty of computing the required differentials to solve the necessary conditions is substantial.

Another interesting issue is the optimization of tracking performance when the signal's SNR is not known. In this case, several ROC curves are involved and one must select a threshold that is best (in some sense) for a whole range of SNRs. Alternatively, an adaptive scheme could be devised, whereby the SNR is monitored and the threshold adjusted so as to maximize q_2 along the current ROC curve.

6. APPLICATION TO MODIFIED LIKELIHOOD FUNCTION

Calculation of the modified likelihood function [18] requires the second moment $\underline{U}_2(m)$ of the combined innovation (10), conditioned on Y^{k-1} and m. This may be written as

$$\underline{U}_2(m) = q_2(m)\underline{S} \tag{33}$$

where $q_2(m)$ represents all the scalar factors on the right-hand side of (23).

Since this is proportional to the single-measurement innovation covariance matrix $\underline{S}$, the standard likelihood function machinery need only incorporate the scale factor $q_2(m)$ in order to compute the modified version. Values of $q_2(m)$ for various m, g, P_D, and C may be precomputed, using the methods described in Section 3 above.

7. CONCLUSION

We have explored an important connection between data association/tracking algorithms and the upstream signal processing/detection algorithms that provide their measurements. A quantitative relationship has been derived that specifies the effect on tracking performance of threshold-dependent parameters such as the probabilities of detection and false alarm, and a graphical technique has been described for selecting an optimal threshold.

THIS PAGE UNINTENTIONALLY LEFT BLANK

APPENDIX A
PROBABILITY CALCULATIONS

In this appendix we shall derive a number of expressions needed in the main text. Letting $\gamma_j(m)$ denote the prior probability of the event χ_j, conditioned on m, the total probability theorem yields

$$\gamma_j(m) = P\{\chi_j|m,Y^{k-1}\} = P\{\chi_j|m\}$$

$$= P\{\chi_j|m^F=m-1,m\}P\{m^F=m-1|m\} + P\{\chi_j|m^F=m,m\}P\{m^F=m|m\}$$

$$= \begin{cases} (1/m)P\{m^F=m-1|m\} + (0)P\{m^F=m|m\}, & j=1,\ldots m \\ (0)P\{m^F=m-1|m\} + (1)P\{m^F=m|m\}, & j=0 \end{cases} \quad (34)$$

because m^F, the number of false measurements, must be either m-1 (if the target is detected) or m (if it is not). Using Bayes' rule and the assumed Poisson distribution for false measurements,

$$P\{m^F=m-1|m\} = P\{m|m^F=m-1\}P\{m^F=m-1\}/P\{m\}$$

$$= [P_D P_G][e^{-CV}(CV)^{m-1}/(m-1)!]/P\{m\}$$

$$= P_D P_G m/[P_D P_G m + (1-P_D P_G)CV] \quad (35)$$

$$P\{m^F=m|m\} = P\{m|m^F=m\}P\{m^F=m\}/P\{m\}$$

$$= [1-P_D P_G][e^{-CV}(CV)^m/m!]/P\{m\}$$

$$(1-P_DP_G)CV/[P_DP_Gm + (1-P_DP_G)CV] \tag{36}$$

where the denominator $P\{m\}$ is the prior probability of m and is equal to the sum of the numerators in the two equations:

$$\begin{aligned} P\{m\} &= P\{m|Y^{k-1}\} \\ &= [P_DP_Gm + (1-P_DP_G)CV]e^{-CV}(CV)^{m-1}/m!, \quad m=0,1,... \end{aligned} \tag{37}$$

Substituting back into (34) yields

$$\gamma_j(m) = \begin{cases} P_DP_G/[P_DP_Gm + (1-P_DP_G)CV], & j=1,...m \\ (1-P_DP_G)CV/[P_DP_Gm + (1-P_DP_G)CV], & j=0 \end{cases} \tag{38}$$

Note that $\gamma_j(m)$ is independent of j for $j>0$.

Using Bayes' rule, the posterior probabilities in (10) can be expressed as

$$\begin{aligned} \beta_j \triangleq P\{\chi_j|Y^k\} &= P\{\chi_j|\underline{\tilde{Y}}_1,...\underline{\tilde{Y}}_m,m,Y^{k-1}\} \\ &= p(\underline{\tilde{Y}}_1,...\underline{\tilde{Y}}_m|\chi_j,m,Y^{k-1})P\{\chi_j|m,Y^{k-1}\}/p(\underline{\tilde{Y}}_1,...\underline{\tilde{Y}}_m|m,Y^{k-1}) \\ &= p(\underline{\tilde{Y}}_1,...\underline{\tilde{Y}}_m|\chi_j,m,Y^{k-1})\gamma_j(m)/\sum_{j=0}^{m} \text{numerators} \end{aligned} \tag{39}$$

The first factor is the joint probability density of the m

candidate measurements, conditioned on the j-th one being correct. According to the PDA assumptions, the correct measurement $\tilde{\underline{Y}}_j$ has a gaussian density

$$N(\tilde{\underline{Y}}_j;\underline{0},\underline{S})/P_G \triangleq (1/P_G)\exp(-\tilde{\underline{Y}}_j'\underline{S}^{-1}\tilde{\underline{Y}}_j/2)/(2\pi)^{M/2}|\underline{S}|^{1/2} \tag{40}$$

with mean $\underline{0}$ and covariance $\underline{S}$, where the factor $1/P_G$ accounts for its restriction to the validation gate, and each incorrect measurement has a uniform density V^{-1}. It follows that

$$p(\tilde{\underline{Y}}_1,\ldots\tilde{\underline{Y}}_m|\chi_j,m,Y^{k-1}) = \begin{cases} V^{-m+1}N(\tilde{\underline{Y}}_j;\underline{0},\underline{S})/P_G, & j=1,\ldots m \\ V^{-m}, & j=0 \end{cases} \tag{41}$$

The second factor in (39) is the prior probability of χ_j, given by (38). The denominator is the <u>joint prior density</u> of the measurements, conditioned only on m (and the past data),

$$p(\tilde{\underline{Y}}_1,\ldots\tilde{\underline{Y}}_m|m,Y^{k-1}) = \tag{42}$$

$$V^{-m}\gamma_0(m) + V^{-m+1}\sum_{j=1}^{m}(1/P_G)N(\tilde{\underline{Y}}_j;\underline{0},\underline{S})\gamma_j(m)$$

Note that with the above conditioning, the validated measurements are not independent, i.e., (42) is not equal to the product over j of the <u>marginal prior densities</u>

$$p(\tilde{\underline{Y}}_j|m,Y^{k-1}) = V^{-1}[1-\gamma_j(m)] + (1/P_G)N(\tilde{\underline{Y}}_j;\underline{0},\underline{S})\gamma_j(m) \tag{43}$$

Finally, substitution of (38), (41), and (42) into (39) followed by a certain amount of rearrangement yields

$$\beta_j = \frac{\exp(-\underline{y}_j' \underline{S}^{-1} \underline{y}_j / 2)}{b + \sum_{i=1}^{m} \exp(-\underline{y}_i' \underline{S}^{-1} \underline{y}_i / 2)} , \qquad j=1,\ldots m \tag{44}$$

$$\beta_0 = \frac{b}{b + \sum_{i=1}^{m} \exp(-\underline{y}_i' \underline{S}^{-1} \underline{y}_i / 2)} \tag{45}$$

where

$$\begin{aligned} b &\triangleq (2\pi)^{M/2} C |\underline{S}|^{1/2} (1-P_D P_G)/P_D \\ &= (2\pi)^{M/2} (CV/c_M g^M) (1-P_D P_G)/P_D \end{aligned} \tag{46}$$

APPENDIX B
DERIVATION OF U_1 AND U_2 INTEGRALS

In this appendix the expectations

$$U_1(m) \triangleq E\left[\sum_{i=1}^{m} \beta_i \tilde{y}_i \tilde{y}_i' \,|\, m, Y^{k-1}\right] \tag{B-1}$$

and

$$U_2(m) \triangleq E\left[\sum_{i=1}^{m} \beta_i \tilde{y}_i \sum_{j=1}^{m} \beta_j \tilde{y}_j' \,|\, m, Y^{k-1}\right] \tag{B-2}$$

will be evaluated, where β_i is given by (44) and the joint density of $\tilde{y}_1, \ldots \tilde{y}_m$ is (42). In order to simplify the arguments, we shall make use of the fact that S is positive definite and change variables to

$$\zeta_i = S^{-\frac{1}{2}} \tilde{y}_i \,, \quad i = 1, \ldots m \tag{B-3}$$

so that

$$\tilde{y}_i' S^{-1} \tilde{y}_i = \zeta_i' \zeta_i = \|\zeta_i\|^2 \tag{B-4}$$

and

$$\tilde{y}_i \tilde{y}_i' = S^{\frac{1}{2}} \zeta_i \zeta_i' S^{\frac{1}{2}} \tag{B-5}$$

In terms of the new variables ζ_i, the validation gate becomes a sphere $\{\zeta : \|\zeta\|^2 \leq g^2\}$ with volume $c_M g^M \triangleq \hat{v}$; the β_i's can be rewritten as

$$\hat{\beta}_i = \frac{e^{-\frac{1}{2}\|\zeta_i\|^2}}{b + \sum_{j=1}^{m} e^{-\frac{1}{2}\|\zeta_j\|^2}}, \quad i = 1,\ldots m \tag{B-6}$$

where

$$b \triangleq (2\pi)^{M/2}(CV/c_M g^M)(1-P_D P_G)/P_D \tag{B-7}$$

is the same as in (46). Note that the dimensionless quantity CV, the average number of false measurements in the (now spherical) gate, is unaffected by the variable change. The joint density (42) becomes

$$p(\zeta_1,\ldots\zeta_m|m,Y^{k-1}) = \gamma_0(m)\hat{v}^{-m} + \gamma_j(m)\hat{v}^{-m+1} \sum_{i=1}^{m} N(\zeta_i;0,I)/P_G \tag{B-8}$$

if $\|\zeta_i\| \leq g$ for all i, and 0 otherwise.

Using the change of coordinates from $\tilde{y}$ to ζ, expressions (19) through (21) may be reexpressed as follows:

$$E[P_k|m,Y^{k-1}] = WS^{\frac{1}{2}}[\hat{U}_1(m)-\hat{U}_2(m)]S^{\frac{1}{2}}W', \quad m=1,2,... \tag{B-9}$$

$$\hat{U}_1(m) = E[\sum_{i=1}^{m}\hat{\beta}_i\zeta_i\zeta_i'|Z^{k-1},m] = S^{-\frac{1}{2}}U_1(m)S^{-\frac{1}{2}} \tag{B-10}$$

$$\hat{U}_2(m) = E[\sum_{i=1}^{m}\hat{\beta}_i\zeta_i \sum_{j=1}^{m}\hat{\beta}_j\zeta_j'|Z^{k-1},m] = S^{-\frac{1}{2}}U_2(m)S^{-\frac{1}{2}} \tag{B-11}$$

Let D stand for the spherical validation gate region. Then the above two expectations may be written out explicitly as multiple integrals of certain matrices, taken over m copies of D:

$$\hat{U}_1 = \int_D\int_D \cdots \int_D A(\zeta_1,...,\zeta_m)p(\zeta_1,...,\zeta_m)d\zeta_1...d\zeta_m \tag{B-12}$$

$$\hat{U}_2 = \int_D\int_D \cdots \int_D B(\zeta_1,...,\zeta_m)p(\zeta_1,...,\zeta_m)d\zeta_1...d\zeta_m \tag{B-13}$$

where p is the joint innovations density (B-8) with the conditioning suppressed and A,B are M×M matrices described componentwise by

$$A_{pq} = \sum_{i=1}^{m}\hat{\beta}_i\zeta_i^p\zeta_i^q \qquad 1 \le p,q \le M \tag{B-14}$$

$$B_{pq} = \sum_{i,j=1}^{m}\hat{\beta}_i\hat{\beta}_j\zeta_i^p\zeta_j^q \qquad 1 \le p,q \le M \tag{B-15}$$

Here the M-dimensional vector ζ_k has been denoted as $(\zeta_k^1, \zeta_k^2, \ldots, \zeta_k^M)$. The integrals (B-12) and (B-13) are actually mM-fold integrals. Although the complexity of undertaking such a large computation directly would prove formidable, a number of observations show that these integrals have a fairly simple and straightforward structure:

Observation 1. The matrices $\hat{U}_1$ and $\hat{U}_2$ are diagonal.

From the expressions (B-14) and (B-15) one may deduce that off-diagonal elements will integrate out to zero. For when $p \neq q$, both A_{pq} and B_{pq} become odd polynomials of second degree in the variables $\zeta_1^1, \ldots, \zeta_m^M$, with coefficients either single $\hat{\beta}$'s or pairwise products of $\hat{\beta}$'s. Now both the $\hat{\beta}$'s and the two terms of the probability density p in (B-8) are positive functions depending only on $\|\zeta_1\|, \ldots, \|\zeta_m\|$, i.e. they have the same values at antipodal points of a sphere. The odd polynomials from A_{pq} and B_{pq} will have opposite values at antipodal points, so that their contributions to the total integral will cancel.

Physically, this amounts to the observation that off-diagonal elements of the inertia tensor vanish in a principal axis system, for a spherical body with the shape of the validation region and with mass distribution density appropriately defined in terms of the $\hat{\beta}$'s and p.

Observation 2. Integrals of cross terms ($i \neq j$) vanish in the sum (B-15) defining B_{pq}.

From the previous observation, we need only concern ourselves with diagonal entries B_{pp}. Again when $i \neq j$ we have an odd polynomial in the ζ's, and the same arguments as before apply again to show its integral over a sphere, weighted by the density p, must vanish.

From the point of view of the original definition (B-11) of $\hat{U}_2$, we could say that distinct innovations ζ_i, ζ_j are orthogonal: their inner products vanish and do not contribute to the second moment of the combined innovations.

Observation 3. Each term of A or B making a nonvanishing contribution to $\hat{U}_N$, N=1 or 2, has the same value, given explicitly by

$$\eta_N = K \int_0^\sigma \cdots \int_0^\sigma \left[\frac{e^{-\frac{1}{2}r_1^2}}{b + \sum_{j=1}^{m} e^{-\frac{1}{2}r_j^2}} \right]^N \left(C_g \sum_{j=1}^{m} e^{-\frac{1}{2}r_j^2} + C_u \right) r_1^2 \left(\prod_{j=1}^{m} r_j \right)^{M-1} dr_1 \cdots dr_m \tag{B-16}$$

where

$$C_g = C_g(m,M) \triangleq \frac{\gamma_j(m)}{(2\pi)^{M/2} (c_M g^M)^{m-1} P_G} \tag{B-17}$$

$$C_u = C_u(m,M) \triangleq \frac{\gamma_0(m)}{(c_M g^M)^m} \tag{B-18}$$

$$K = K(m,M) = M^{m-1} c_M^m \tag{B-19}$$

To prove this, let us consider the first term of the (1,1) entry of each integral, which can be written as $\hat{\beta}_1^N(\zeta_1^1)^2 p(\zeta_1,\ldots,\zeta_m)$, N=1,2. Since p and $\hat{\beta}_1$ depend only on the norms $||\zeta_i|| = r_i$, it is clearly advantageous to introduce spherical coordinates in each of the m copies of the ζ-space:

$$d\zeta_i = d\zeta_i^1 d\zeta_i^2 \ldots d\zeta_i^M = r_i^{M-1} dr_i d\omega_i^{M-1} \tag{B-20}$$

Here $d\omega_i^{M-1}$ denotes the "unit solid angle," i.e. the surface element on the unit sphere $(\zeta_i^1)^2 + (\zeta_i^2)^2 + \ldots + (\zeta_i^M)^2 = 1$.

Making these substitutions, the integral for the expected value of $\hat{\beta}_1^N(\zeta_1^1)^2$ becomes

$$\int_0^\sigma \cdots \int_0^\sigma \left[\frac{e^{-\frac{1}{2}r_1^2}}{b+\sum_{j=1}^m e^{-\frac{1}{2}r_j^2}}\right]^N (\zeta_1^1)^2 \left(C_g \sum_{j=1}^m e^{-\frac{1}{2}r_j^2} + C_u\right) (r_1^{M-1} dr_1 d\omega_1^{M-1}) \ldots (r_m^{M-1} dr_m d\omega_m^{M-1}) \tag{B-21}$$

The constants C_g, C_u, and K defined in (B-17), (B-18) are introduced to simplify the notation.

The expression in (B-21) is not yet complete because the variable ζ_1^1 still has to be reexpressed in angular ω_1-coordinates for the first copy of the M-dimensional state space. However, the other angular variables $\omega_2^{M-1},\ldots,\omega_m^{M-1}$ do not occur in the integrand, so that their integrals can be absorbed in the constant K. The fact needed to do this is that the integral of the unit solid angle is just the surface area of the unit sphere, which is M times c_M (the volume of the unit sphere).

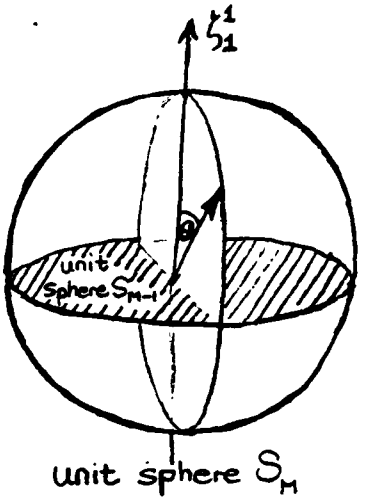

To handle the ζ_1^1-dependence of the integrand in (B-21) we are going to use an argument almost identical to the one used to derive the volume of the unit sphere (which is to start from a known integral and "work backwards"). The known integral that we wish to exploit is

$$\int_{\mathbb{R}_M} (\zeta_1^1)^2 \exp(-\tfrac{1}{2}\sum_{j=1}^{M} \zeta_j^2)\, d\zeta_1^1 d\zeta_1^2 \ldots d\zeta_1^M = (2\pi)^{M/2} \qquad \text{(B-22)}$$

Now if this integral is rewritten in spherical coordinates, we should make a substitution $\zeta_1^1 = r_1 f(\omega_1^{M-1})$ where f is a smooth function independent of r_1. For example if coordinates are chosen on the sphere as depicted in the figure, we would have $f(\omega_1^{M-1}) = \cos\theta$, where the angle θ is measured downward from the north pole as shown. Rewriting (B-22) in spherical coordinates gives

$$(2\pi)^{M/2} = \int_0^\infty r_1^2 e^{-\frac{1}{2}r_1^2}\, r_1^{M-1}\, dr_1 \int_{\substack{\text{sphere} \\ r_1 \equiv 1}} f^2(\omega_1^{M-1})\, d\omega_1^{M-1} \qquad \text{(B-23)}$$

The substitution $\frac{1}{2}r_1^2 = x_1$ transforms the radial part of (B-22) into the well-known integral representation for the gamma function

$$\Gamma(t) = \int_0^\infty e^{-x_1}\, x_1^{t-1} dx_1 \qquad \text{(B-24)}$$

so now we have

$$(2\pi)^{M/2} = 2^{M/2}\Gamma\left(\frac{M}{2} + 1\right) \int_{\substack{\text{sphere} \\ r_1 = 1}} f^2(\omega_1^{M-1})\, d\omega_1^{M-1} \qquad \text{(B-25)}$$

We are now in a position to solve for the nonradial part of the integral in (B-25). But when this is done, the quantity we obtain is recognized to be c_M, the volume of the unit sphere:

$$\int f^2(\omega_1^{M-1})\, d\omega_1^{M-1} = \frac{\pi^{M/2}}{\Gamma(\frac{M}{2}+1)} = c_M \qquad \text{(B-26)}$$

Actually, by using properties of the gamma function, this expression for c_M can be written more explicitly as

$$c_M = \frac{2\pi}{M} c_{M-2} = \begin{cases} \dfrac{2^{M/2}\pi^{M/2}}{M(M-2)\ldots 4\cdot 2} = \dfrac{\pi^{M/2}}{(m/2)!} & \text{if M is even} \\ \dfrac{2^{(M+1)/2}\,\pi^{(M-1)/2}}{M(M-2)\ldots 5\cdot 3\cdot 1} & \text{if M is odd} \end{cases} \qquad \text{(B-27)}$$

Now returning to the original integral (B-21), we note that even though the integrand is <u>not</u> the same as (B-22), the angular dependence <u>is</u>, so that (B-26) may be applied. Absorbing this c_M into K shows that the $\beta_1^N(\zeta_1^1)^2$-contribution to $\hat{U}_N$ is given exactly by (B-16). It should be noted that this formula is also immediately valid for M=1 without even introducing the spherical change of coordinates (B-20), since the volume of the unit interval is 2 (correctly given by B-27).

Although we began the discussion by considering the contribution of a single term $\hat{\beta}_1^N(\zeta_1^1)^2$ to the expectation, the

homogeneity of the expression (B-21) shows that the other terms $\hat{\beta}_1^N(\zeta_1^2)^2,\ldots,\hat{\beta}_M^N(\zeta_1^M)^2$ in the (1,1)-entry will each make an identical contribution. The same argument applies to other diagonal entries of $\hat{U}_1$ and $\hat{U}_2$: homogeneity again shows that each term will make the same contribution, given by (B-16). This justifies the conclusion that

$$\hat{U}_N = m\eta_N I \tag{B-28}$$

where I is the identity matrix.

Next, let us transform back from ζ-coordinates to the original ν-coordinates as given in (B-5). We have proven that our original expectations U_1, U_2 are scalar multiples of the covariance matrix S:

$$U_N = S^{\frac{1}{2}}(m\eta_N I)S^{\frac{1}{2}} = m\eta_N S \tag{B-29}$$

Finally, substitution of (B-17)-(B-19) and (38) into (B-16) followed by numerous cancellations yields the expressions (22)-(25) in Section 3.

REFERENCES

1. R. E. Kalman and R. S. Bucy, "New Results in Filtering and Prediction Theory," Trans. ASME: J. Basic Eng., Vol. 83, March 1961, pp. 95-108.

2. I. B. Rhodes, "A Tutorial Introduction to Estimation and Filtering," IEEE Trans. Auto. Control, Vol. AC-16, December 1971, pp. 688-706.

3. A. H. Jazwinski, Stochastic Processes and Filtering Theory, Academic Press, 1970.

4. P. S. Maybeck, Stochastic Models, Estimation, and Control -- Volume 1, Academic Press, 1979.

5. B. D. O. Anderson and J. B. Moore, Optimal Filtering, Prentice-Hall, 1979.

6. Y. Bar-Shalom and E. Tse, "Tracking in a Cluttered Environment with Probabilistic Data Association," Automatica, Vol. 11, September 1975, pp. 451-460.

7. T. E. Fortmann and S. Baron, "Problems in Multi-Target Sonar Tracking," Proc. 1978 IEEE Conf. on Decision and Control, San Diego, California, January 1979.

8. T. E. Fortmann, Y. Bar-Shalom, and M. Scheffe, "Multi-Target Tracking Using Joint Probabilistic Data Association," Proc. 1980 IEEE Conference on Decision and Control, Albuquerque, New Mexico, December 1980.

9. R. Singer, R. Sea, and K. Housewright, "Derivation and Evaluation of Improved Tracking Filters for use in Dense Multitarget Environments," IEEE Trans. Info. Theory, Vol. IT-20, July 1974, pp. 423-432.

10. D. B. Reid, "An Algorithm for Tracking Multiple Targets," IEEE Trans. Auto. Control, Vol. AC-24, December 1979, pp. 843-854.

11. E. Taenzer, "Tracking Multiple Targets Simultaneously with a Phased Array Radar," IEEE Trans. Aerospace and Electronic Systems, Vol. AES-16, September 1980, pp. 604-614.

12. C. L. Morefield, "Application of 0-1 Integer Programming to Multitarget Tracking Problems," IEEE Trans. Auto. Control, Vol. AC-22, June 1977, pp. 302-312.

13. D. L. Alspach, "A Gaussian Sum Approximation to the Multitarget Identification - Tracking Problem," Automatica, Vol. 11, May 1975, pp. 285-296.

14. R. W. Sittler, "An Optimal Data Association Problem in Surveillance Theory," IEEE Trans. Mil. Electron., Vol. MIL-8, April 1964, pp. 125-139.

15. Y. Bar-Shalom, "Tracking Methods in a Multi-Target Environment," IEEE Trans. Auto. Control, Vol. AC-23, August 1978, pp. 618-626.

16. H. L. Wiener, W. W. Willman, I. R. Goodman, and J. H. Kullback, "Naval Ocean-Surveillance Correlation Handbook, 1978," NRL Report 8340, Naval Research Lab, October 1979.

17. I. R. Goodman, H. L. Wiener, and W. W. Willman, "Naval Ocean-Surveillance Correlation Handbook, 1979," NRL Report 8402, Naval Research Laboratory, September 1980.

18. T. E. Fortmann and Y. Bar-Shalom, "Modification of the Likelihood Function to Account for Probabilistic Data Association," BBN Report 3964A (revised), Bolt Beranek and Newman Inc., November 1979, Contract N00039-78-C-0296.

19. H. Urkowitz, "Energy Detection of Unknown Deterministic Signals," Proc. IEEE, Vol. 55, No. 4, April 1967, pp. 523-531.

20. A. D. Whalen, Detection of Signals in Noise, Academic Press, 1971.

DISTRIBUTION LIST
FOR
"DETECTION THRESHOLDS FOR MULTI-TARGET TRACKING IN CLUTTER"

All addressees receive one copy unless otherwise specified.

Defense Technical Information Center
Cameron Station
Alexandria, VA 22314 — 12 copies

Center for Naval Analyses
2000 North Beauregard Street
Alexandria, VA 22311

Adphatech, Inc.
260 Hillside Avenue
Arlington, MA 02174

Defense Advanced Research Projects Agency
Tactical Technology Office
1400 Wilson Boulevard
Arlington, VA 22209

Office of Naval Research
800 N. Quincy Street
Arlington, VA 22217
Code 434 — 2 copies
Code 436

Dr. Byron D. Tapley
The University of Texas at Austin
Department of Aerospace Engineering
and Engineering Mechanics
Austin, TX 78712

Dr. Fred W. Weidmann
Tracor, Inc.
Tracor Sciences & Systems
6500 Tracor Lane
Austin, TX 78721

Dr. Richard L. Moose
Virginia Polytechnic Institute
and State University
Department of Electrical Engineering
Blacksburg, VA 24061

Daniel H. Wagner Associates
Station Square One
Philadelphia, PA 19301

Massachusetts Institute of Technology
Laboratory for Information and Decision
Systems
Cambridge, MA 02139

Xybion Corporation
7 Ridgedale Avenue
Cedar Knolls, NJ 07927

Orincon Corporation
3366 North Torrey Pines Court
Suite 320
LaJolla, CA 92037 — 2 copies

Dr. George Johnson
IBM
Federal Systems Division
9500 Godwin Drive
Manassas, VA 22110

Dr. Nasser Ahmid
Kansas State University
Department of Electrical Engineering
Manhattan, KS 66506

Naval Postgraduate School
Monterey, CA 93940
Dr. H. Titus
Dr. N. Forrest
Dr. G. Sackman

DARPA Research Center
Unit #1
Moffett Field, CA 94035

Naval Underwater Systems Center
Code 352
Code 356
Newport, RI 02840

Analysis and Technology, Inc.
P. O. Box 220
North Stonington, CT 06359

Planning Systems, Inc.
7900 West Park Drive
McLean, VA 22101

DISTRIBUTION LIST (Cont'd)

Dr. J. Anton
Systems Control, Inc.
1801 Page Mill Road
Palo Alto, CA 94304

Office of Naval Research Eastern
Regional Office
666 Summer Street
Boston, MA 02210

Dr. Thomas O. Mottl
The Anlytic Science Corporation
Six Jacob Way
Reading, MA 01867

VERAC, Inc.
4901 Morena Boulevard
Suite 209
San Diego, CA 92117

Bolt, Beranek and Newman, Inc.
3065 Rosecrans Place
San Diego, CA 92110

Naval Surface Weapons Center
White Oak Laboratory
Code U-20
Silver Spring, MD 20910 2 copies

Dr. Yaakov Bar-Shalom
The University of Connecticut
Department of Electrical Engineering
and Computer Science
Box U-157
Storrs, CT 06268

Naval Ocean Systems Center
Code 632
Code 7319
San Diego, CA 92152

Dr. C. Carter
Naval Underwater Systems Center
New London Laboratory
Code 313
New London, CT 06320

Naval Air Development Center
Code 203
Warminster, PA 18974

Naval Electronic Systems Command
Washington, D.C. 20360
Code 320
Code 350
PME-124

Manager, ASW Systems Project Office
Naval Material Command
ASW-118
Washington, D.C. 20360

Naval Research Laboratory
Washington, D.C. 20375
Code 2627
Code 5308
Code 7932

Naval Sea Systems Command
Washington, D.C. 20360
Code 63R-1
Code 63R-16
Code 63D (R. Cockerill)
Code 63D (A. Anderson)

Professor John Dennis
Rice University
Department of Mathematical Sciences
Houston, TX 77001

Professor Fred Fisher
Marine Physical Laboratory
Scripps Institute of Oceanography
San Diego, CA 92152

Mr. J. W. Conrad
Naval Intelligence Support Center
Code 20C
Suitland, MD 20390

Mr. V. T. Gabriel
General Electric Company
Sonar Systems Engineering
Farrell Road Plant
Building 1, Room D6
Syracuse, NY 13201

Dr. C. B. Chang
Lincoln Lab/MIT
Lexington, MA 02173

ATAC, Inc.
P. O. Box 62199
Sunnyvale, CA 94088


DATE
ILMF